Energy transfer relation of a novel $Ce^{3+}/Pr^{3+}/Eu^{3+}$ co-doped $Sr_{2.975-x}La_xAlO_{4+x}F_{1-x}$ solid solution phosphor*

Wang Yan-Ze(王延泽), Ma Jian(马 健), Sun Liang(孙 亮), Li Rui(李 蕊), and Wang Da-Jian(王达健)†

Institute of Materials Physics, School of Materials Science and Engineering, Tianjin University of Technology, Tianjin 300384, *China*

(Received 7 March 2014; revised manuscript received 22 April 2014; published online 20 August 2014)

The photoluminescence properties and energy transfer of a new Ce^{3+}/ Pr^{3+}/ Eu^{3+} co-doped solid-solution composition of $Sr_{2.975-x}La_xAlO_{4+x}F_{1-x}$ (LSAF) phosphor are investigated. Upon doping Pr^{3+} into lattices of LSAF:Ce host, a shoulder emission peak is observed at about 620 nm, owing to the transition of $^1D_2 \rightarrow {}^3H_4$. Addition of Eu^{3+} to LSAF:Ce^{3+}, Pr^{3+} phosphor results in a sharp emission peaked at 675 nm for the $^5D_0 \rightarrow {}^7F_3$ transition and an increase of the intensity of red emission for Pr^{3+} with increasing Eu^{3+} concentration. The pathways of energy transfer among Ce^{3+}, Pr^{3+}, and Eu^{3+} are proposed to be responsible for color addition of a red component to the primary yellow emission, enabling a potential adjustable color for blue excitable warm white.

Keywords: energy transfer, solid solution, red emission, phosphor

PACS: 78.55.–m **DOI:** 10.1088/1674-1056/23/10/107805

1. Introduction

Typical high efficiency phosphor-converted (PC) white light emitting diodes (LEDs) were fabricated through combining the yellow emitting $Y_3Al_5O_{12}$:Ce^{3+} (YAG:Ce^{3+}) phosphor with blue InGaN LEDs to achieve low cost, high brightness, and ease of fabrication.[1,2] However, the lower color rendering index (CRI) and color reproducibility[3,4] of the phosphors have restrained the application of the illumination devices for white quality. Therefore, the development of suitable color converters is of utmost importance to enable the color to be tunable. The solid solution phosphor system has such an advantage in its adjustable composition photoluminescence, and the typical solid solution phosphor can be exemplified by a Sialon-based phosphor.[5,6] Such a very promising blue excitable solid solution phosphor system was reported recently by Im *et al.*[7–9] A series of solid solutions between the phosphor host compounds of Sr_3AlO_4F and Sr_3SiO_5 and those of $LaSr_2AlO_5$ and Sr_3SiO_5, as well as the phosphor host from the solid solutions of $GdSr_2AlO_5$ and Sr_3AlO_4F, exhibits attractive optical properties and competitive cost. No more attention, however, has been paid to this variety of phosphor. We herein propose a new variety of solid solutions between the isostructural phosphor host compounds $LaSr_2AlO_5$ (LSA) and Sr_3AlO_4F (SAF). The phosphor is chosen to have the formula $Sr_{2.975-x}La_xAlO_{4+x}F_{1-x}$:$0.025Ce^{3+}$ (LSAF:Ce^{3+}, $x = 0$, 0.1, 0.3, 0.5, 0.7, 0.9, 1). We explore the possibility of emission color tuning by using rare-earth ion (Ce^{3+}, Pr^{3+}, Eu^{3+}) singly doped or co-doped LSAF phosphors, and investigate their luminescence and energy transfer properties in detail.

2. Experiment

The powder samples were prepared by a high-temperature solid-state synthesis procedure. The raw materials of La_2O_3, $SrCO_3$, Al_2O_3, SrF_2, CeO_2, Pr_2O_3, and Eu_2O_3 in a general formula of $Sr_{2.475}Ce_{0.025}La_{0.5}AlO_{4.5}F_{0.5}$:$yPr^{3+}$, zEu^{3+} ($y = 0$, 0.02, 0.04, 0.06, 0.08; $z = 0$, 0.01, 0.02, 0.03, 0.04 in atomic fraction) were weighed then mixed well. After grinding in an agate mortar, the mixture was subjected to firing at 1300° in a reducing atmosphere of 8%H_2/92%N_2 for 4 h.

The crystallographic data of as-prepared samples were investigated by X-ray power diffraction (XRD) on a diffractometer (Rigaku D/max-2500/p c, Japan) with a graphite monochromator using Cu-Kα radiation ($\lambda = 0.154062$ nm). The photoluminescence (PL) and photoluminescence of excitation (PLE) spectra of samples were recorded on a fluorescence spectrometer equipped with a xenon light source (Hitachi F-4600, Japan). All of these measurements were made at room temperature.

3. Results and discussion

3.1. LSAF:Ce^{3+} phosphor

3.1.1. Phase and crystal cell evolution of the solid solution phosphor LSAF:Ce^{3+}

It has been recognized that SAF belongs to the Cs_3CoCl_5 structural family with a tetragonal space group $I4/mcm$.[10]

*Project supported by the National Natural Science Foundation of China (Grant Nos. 21076161 and 50872091).

†Corresponding author. E-mail: djwang@tjut.edu.cn

© 2014 Chinese Physical Society and IOP Publishing Ltd

The SAF lattice is composed of $[Sr1_2F]^{3+}$ layers (zSr1 = 0 or 1/2) alternating with $[Sr_2AlO_4]^{3-}$ layers (zSr2 = zAl = 1/4 or 3/4) along the c axis, as shown in Fig. 1(a). The LSA:Ce^{3+} lattice is composed of $[(La/Sr1)O]^{3+}$ layers (zLa = zSr1 = 0 or 1/2) alternating with $[Sr_2AlO_4]^{3-}$layers (zSr2 = zAl = 1/4 or 3/4) along the c axis, as shown in Fig. 1(b).[11] The two compounds have similar crystal structures of the main group element.

Figure 2 displays the evolution of XRD patterns of LSAF:Ce^{3+} (x = 0, 0.1, 0.3, 0.5, 0.7, 0.9, 1.0). The diffraction patterns of all samples were similar to those of $LaSr_2AlO_5$ or Sr_3AlO_4F with varied x values, proving that the LSAF:Ce^{3+}solid is formed. An enlargement of the strongest diffraction peak of the phosphors at $2\theta = 30°$ shows a distinct peak shift. The peak shifts to lower scattering angle with increasing x, which can be attributed to the replacement of larger Sr^{2+} (R_{Sr} = 1.26 Å) by the smaller La^{3+} (R_{La} = 1.16 Å) concurrent to the replacement of the smaller F^- (R_F = 1.31 Å) by the larger O^{2-} (R_O = 1.38 Å).

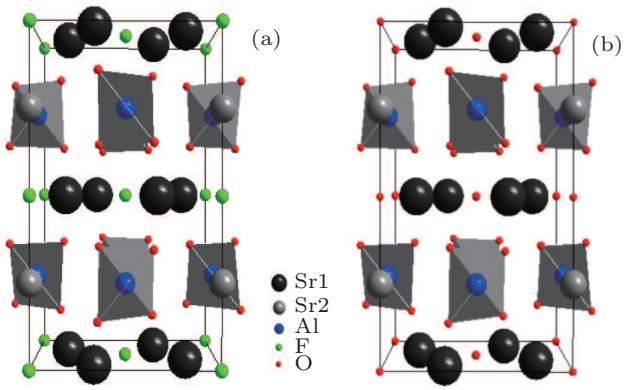


Fig. 1. (color online) (a) Unit-cell representative of Sr_3AlO_4F. (b) The crystal structure of $LaSr_2AlO_5$:Ce^{3+}. The atoms in order of size from large to small represent Sr1, Sr2, Al, F, and O, respectively.

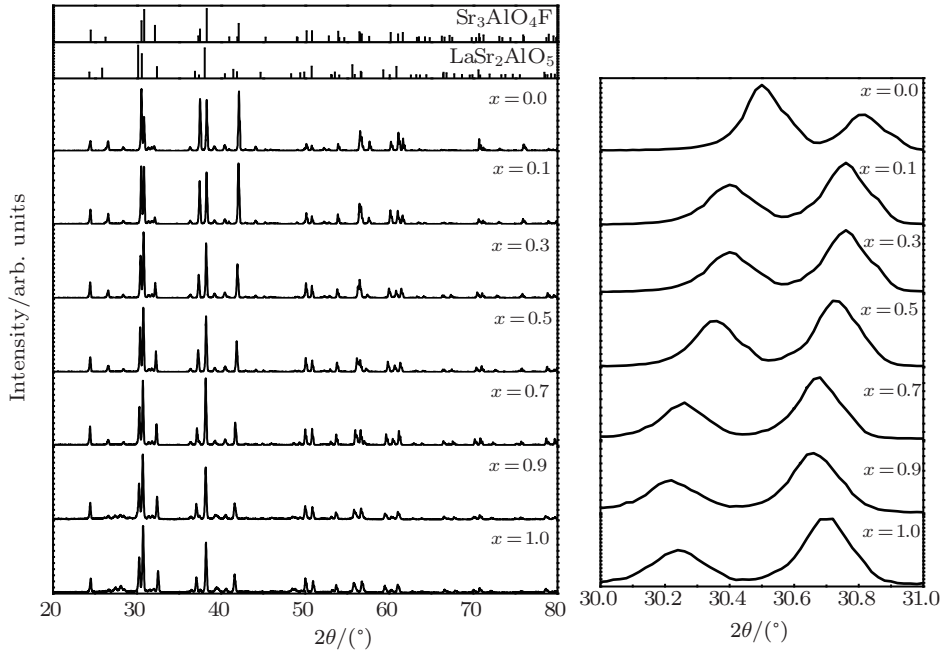


Fig. 2. XRD patterns of $Sr_{2.975-x}La_xAlO_{4+x}F_{1-x}$:0.025$Ce^{3+}$ (LSAF:Ce^{3+}) for x = 0, 0.1, 0.3, 0.5, 0.7, 0.9, 1.

3.1.2. PL properties of LSAF:Ce phosphor

Figure 3(a) shows PL (emission) and PLE (excitation) spectra of $Sr_{2.975-x}La_xCe_{0.025}AlO_{4+x}F_{1-x}$ (x = 0.3) phosphor. The emission spectrum exhibits a broad profile with a maximum at about 527 nm, owing to the 5d→4f transition at the Ce^{3+} centers. The dependences of peak position and intensity on x in LSAF:Ce^{3+} are displayed in Fig. 3(b). With increasing x value in LSAF:Ce^{3+}, more oxygen ions replace the fluorine ions and the emission peak positions gradually shift to longer wavelengths from 498 nm for Sr_3AlO_4F:Ce^{3+} (x = 0) to 553 nm for $LaSr_2AlO_5$:Ce^{3+} (x = 0.7). This shift is attributed to an increase of the lattice covalence because oxides tend to have a greater centroid shift of the d orbitals than fluorides, leading to an emission red shift.[12–15] From Fig. 3(b), we observe that the optimum emission of Ce^{3+} is at x = 0.3 for LSAF:Ce^{3+}. As the x value increases beyond 0.3, a drop in emission intensity is observed. Due to a broad yellow emission and intense excitation band present in the visible spectral region, LSAF:Ce^{3+} can be applied to white LEDs pumped by blue LEDs or near-UV LEDs.

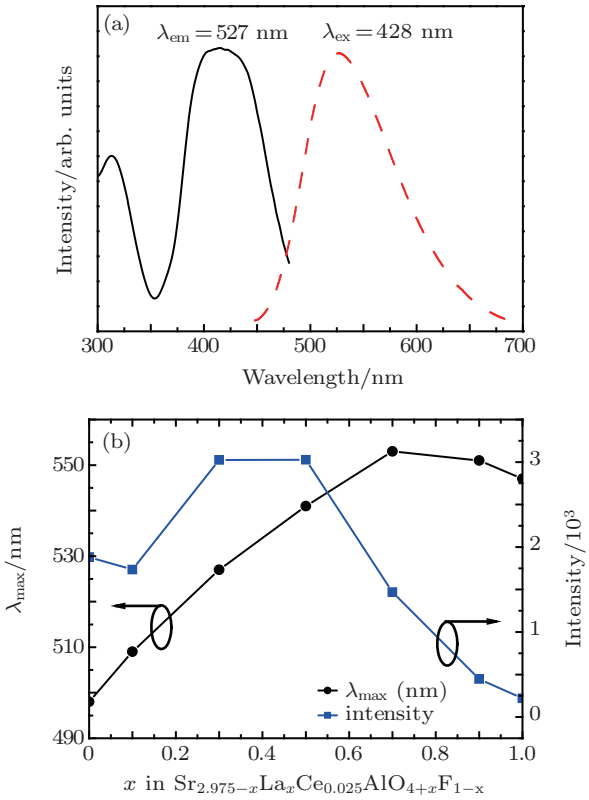


Fig. 3. (color online) The PLE (excitation) and PL (emission) spectra of $Sr_{2.975-x}La_xCe_{0.025}AlO_{4+x}F_{1-x}$ ($x = 0.3$) (a) and the wavelength positions of the emission maximum and luminescence intensity varying with x in LSAF:Ce^{3+} (b).

3.2. Pr^{3+}-, Eu^{3+}-doped LSAF:Ce^{3+} phosphor

3.2.1. XRD analysis

The compositions and phase purities of the samples were investigated by XRD. Figure 4 shows the representative XRD patterns for LSAF:Ce^{3+}, LSAF:Pr^{3+}, LSAF:Eu^{3+}, LSAF:Ce^{3+}, Pr^{3+}, LSAF:Ce^{3+}, Eu^{3+}, and LSAF:Ce^{3+}, Pr^{3+}, Eu^{3+} samples each annealed at 1300 °C in H_2/N_2 for 4 h. No impurity phases were detected, indicating that the RE^{3+} ions are completely incorporated into the LSAF host lattice and its primary crystal structure remains unchanged in its lattice frame.

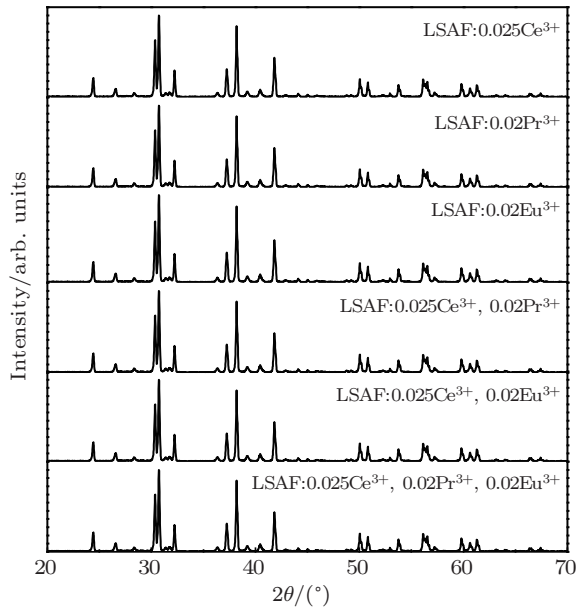


Fig. 4. Representative XRD patterns of LSAF:0.025Ce^{3+}, LSAF: 0.02Pr^{3+}, LSAF: 0.02Eu^{3+}, LSAF: 0.025Ce^{3+}, 0.02Pr^{3+}, LSAF: 0.025Ce^{3+}, 0.02Eu^{3+}, and LSAF: 0.025Ce^{3+}, 0.02Pr^{3+}, 0.02Eu^{3+} samples.

3.2.2. PL properties of Pr^{3+}-, Eu^{3+}-doped LSAF:Ce^{3+} phosphor

In order to improve CRI of LSAF:Ce phosphor by enhancing emission intensity in the red spectral region, red emission needs to be added to the broad yellow emission. There are two typical red emitting activators, Eu^{3+} and Pr^{3+}, for this purpose.[16–18] Figure 5 shows the PL and PLE spectra of Ce^{3+}, Pr^{3+}, Eu^{3+} singly (Figs. 5(a)–5(c), doubly (Figs. 5(d) and 5(e)), and triply (Fig. 5(f)) doped LSAF ($x = 0.5$). The Ce^{3+} singly doped sample exhibits a well-known yellow emission band peaked at around 535 nm due to the transition from the lowest-lying 5d state to the 4f ground state of Ce^{3+}. The PLE spectrum of the yellow band consists of a band at 430 nm corresponding to the transition from the ground state to the lowest-lying 5d state, and an ultraviolet (UV) PLE band corresponding to the upper 5d state, located at 320 nm as shown in Fig. 5(a). The Pr^{3+} singly doped sample exhibits five emission bands upon 286-nm excitation, as shown in Fig. 5(b). The emission bands in the UV region contain one strong band located at 380 nm and originate from the transitions from the lowest-lying 4f5d state to ^3F_J ($J = 2, 3, 4$).[19] The band in the range of 450 nm–600 nm consists of one blue emission band with a maximum at 495 nm, which originates from the $^3P_0 \rightarrow {}^3H_4$ transition, and the other yellow emission band located at 545 nm due to the $^3P_0 \rightarrow {}^3H_5$ transition. The emission band in the red region originates from the $^1D_2 \rightarrow {}^3H_4$ transition dominated by an intense emission line at 620 nm, and a weak satellite line at 660 nm due to $^3P_0 \rightarrow {}^3F_2$.[20,21] The PLE spectra of the 'Pr^{3+} singly doped sample are peaked at 286 nm and 238 nm. In Fig. 5(c), the excitation spectrum of LSAF:Eu^{3+} can be divided into two parts: one part is from 230 nm to 350 nm with a maximum at 306 nm, which is attributed to the charge transfer band (CTB) of O^2–Eu^{3+};[22] the other part, from 350 nm to 500 nm, consists of f–f transitions of Eu^{3+} ions. The major red emission peak of the LSAF:Eu^{3+} sample is located at 620 nm, together with some weak peaks assigned to $^5D_0 \rightarrow {}^7F_1$, $^5D_0 \rightarrow {}^7F_2$, $^5D_0 \rightarrow {}^7F_3$, and $^5D_0 \rightarrow {}^7F_4$ in a range from 500 nm to 700 nm.[23] In Fig. 5(d), the PL spectra of the Ce^{3+} and Pr^{3+} doubly doped sample consist of the yellow band of Ce^{3+} and the red band of Pr^{3+} peaked at 620 nm upon 400 nm excitation. In Fig. 5(e), the PL spectra of the Ce^{3+} and Eu^{3+} doubly doped sample exhibit Eu^{3+} typical emission at 675 nm due to the $^5D_0 \rightarrow {}^7F_3$ transitions and Ce^{3+} yellow emission at 550 nm upon 450-nm excitation. The

PL spectrum of the triply doped sample exhibits all the typical emissions of Ce^{3+}, Pr^{3+}, and Eu^{3+}, and emission peaks are located respectively at 550 nm, 620 nm, and 675 nm under the 450-nm excitation, as shown in Fig. 5(f).

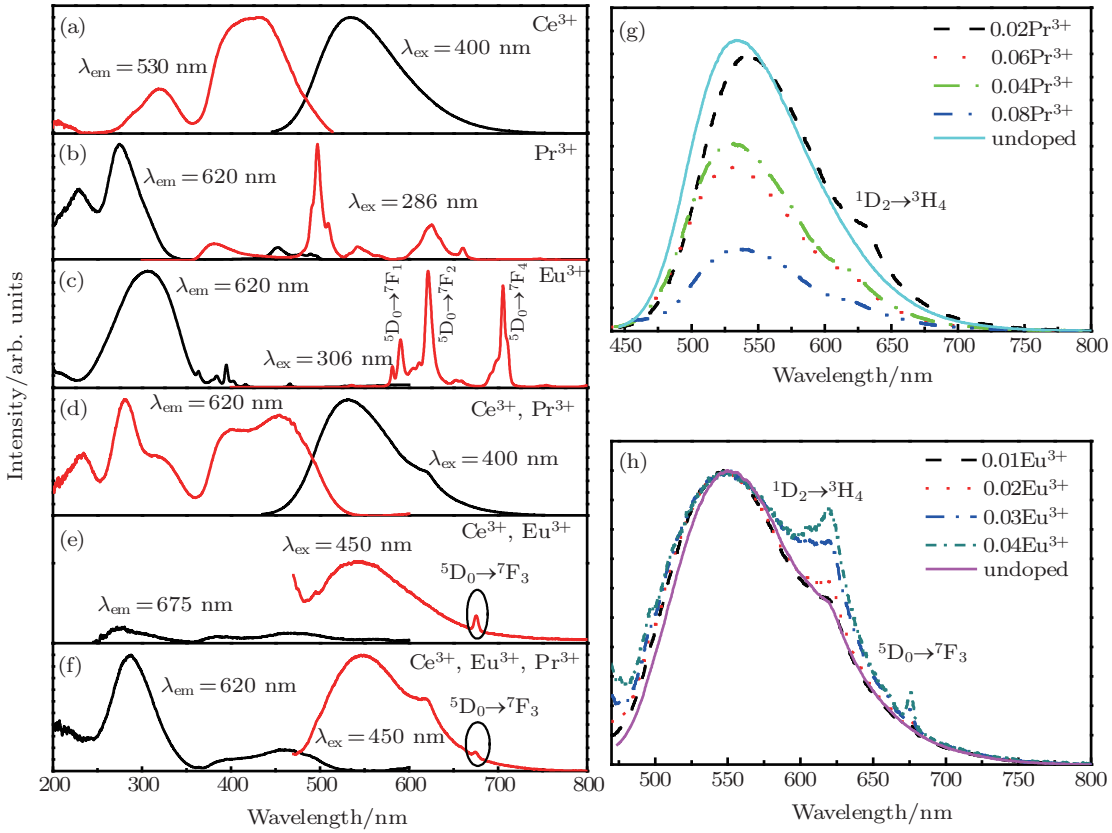


Fig. 5. (color online) PLE excitations and PL emission spectra of LSAF:0.025Ce^{3+} (a), LSAF:0.02Pr^{3+} (b), LSAF:0.02Eu^{3+} (c), LSAF:0.025Ce^{3+}, 0.02Pr^{3+} (d), LSAF:0.025Ce^{3+}, 0.02Eu^{3+} (e), LSAF:0.025Ce^{3+}, 0.02Eu^{3+}, 0.02Pr^{3+} (f), LSAF:0.025Ce^{3+}, $x$$Pr^{3+}$ (x = 0, 0.02, 0.04, 0.06, 0.08) (g), and LSAF:0.025Ce^{3+}, 0.02Pr^{3+}, $y$$Eu^{3+}$ (y = 0, 0.01, 0.02, 0.03, 0.04) (h).

3.2.3. Energy transfer among Ce^{3+}, Pr^{3+}, and Eu^{3+} in LSAF host

As the Pr^{3+} content increases in the LSAF:Ce, Pr phosphors, the intensities of both Ce^{3+} emission and Pr^{3+} emission decrease, as shown in Fig. 5(g). There are two possible mechanisms behind these phenomena. One is a structural change of phase with increasing Pr^{3+} content in the LSAF host lattice and the other is an increase of energy transfer from Ce^{3+} to Pr^{3+}. From the XRD patterns shown in Fig. 4, it is clear that no impurity phase forms when increasing Pr^{3+} content up to 0.08 mole fraction. Therefore, it is believed that the decrease of the yellow emission of Ce^{3+} is due to an energy transfer from Ce^{3+} to Pr^{3+}. From the energy level diagrams shown in Fig. 6 it follows that the energy transfer takes place from the relaxed lowest 5d energy band of Ce^{3+} to the $^1D_2$ energy level of Pr^{3+}. In Fig. 5(d), the PL spectra of the Ce^{3+} and Pr^{3+} doubly doped sample contain not only the yellow band of Ce^{3+} but also the red bands of Pr^{3+} when only Ce^{3+} is excited at 400 nm. Furthermore, the PLE spectrum monitoring Pr^{3+} 620 nm emission includes two typical Ce^{3+} absorption bands at 400 nm and 320 nm, demonstrating the occurrence of Ce^{3+} →Pr^{3+} energy transfer. In Fig. 5(e), the PL spectrum of the Ce^{3+} and Eu^{3+} doubly doped sample exhibits Eu^{3+} typical emission at 675 nm and Ce^{3+} yellow emission at 550 nm when Ce^{3+} is only excited by 450 nm, and the PLE spectrum monitoring the Eu^{3+} emission shows a clear Ce^{3+} absorption band at 450 nm, indicating the Ce^{3+} →Eu^{3+} energy transfer. Furthermore, the LSAF:Eu^{3+} sample does not emit visible light under the 450 nm excitation and its effective excitation peaks are located in a 200 nm–400 nm region, as shown in Fig. 5(c), which can be explained by the fact that in the LSAF:Ce^{3+}, Eu^{2+} sample only a peak at 675 nm could be observed. Figure 5(h) shows the PL spectra of the Ce^{3+}, Pr^{3+}, Eu^{3+} triply doped sample with variable Eu^{3+} concentration in a range of 0 mol–0.04 mol upon 450 nm excitation. All spectra are normalized to the yellow band. The red band emission intensity of Pr^{3+} increases with the augmentation of Eu^{3+} concentration, indicating an increase of the Eu^{3+} →Pr^{3+} energy transfer efficiency. As described above, there exist energy transfer paths of Ce^{3+}–Pr^{3+}, Ce^{3+}–Eu^{3+}, and Eu^{3+}–Pr^{3+} in the Ce^{3+},

Pr^{3+} and Eu^{3+} triple-doped LSAF sample. When the upper 5d state of Ce^{3+} is excited at 450 nm, a rapid relaxation down to the lowest 5d state occurs, and then energy transfer takes place subsequently from Ce^{3+} to Pr^{3+} and from Ce^{3+} to Eu^{3+}, followed by transferring energy from Eu^{3+} to Pr^{3+}, which is described in the transfer pathway diagrams in Fig. 6.

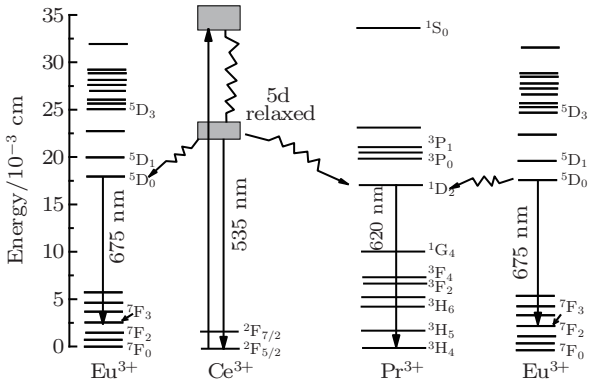


Fig. 6. Proposed energy diagrams showing that the energy transfer takes place among Ce^{3+}, Pr^{3+}, and Eu^{3+} in the LSAF host lattice.

4. Conclusions

In this paper, we presented a new composition of LSAF:Ce^{3+} solid solution phosphors from the end members containing $LaSr_2AlO_5$ and Sr_3AlO_4F. By slightly tuning the inter-atomic distance and ionic characteristic of the host lattice through adding co-dopants, the emission wavelength peak of the phosphor is sensitive to the shift from 498 nm to 553 nm. Doping with Pr^{3+} and Eu^{3+} leads to sharp emissions peaked at 620 nm and 675 nm in the red region. Effective energy transfer of $Ce^{3+} \rightarrow Pr^{3+}$ and $Ce^{3+} \rightarrow Eu^{3+} \rightarrow Pr^{3+}$ are responsible for intensifying the red emission. In terms of adjustable color in the red region, this $Ce^{3+}/Pr^{3+}/Eu^{3+}$co-doped LSAF phosphor provides a simple means to increase the color rendering index for warm white LEDs.

References

[1] Schlotter P, Schmidt R and Schneider J 1997 *Appl. Phys. A: Mater. Sci. & Process.* **64** 417
[2] Oh J R, Cho S H, Lee Y H and Do Y R 2009 *Opt. Express* **17** 7450
[3] Chen Y B, Gong M L, Wang G and Su Q 2007 *Appl. Phys. Lett.* **91** 071117
[4] Jang H S, Im W B, Lee D C, Jeon D Y and Kim S S 2007 *J. Lumin.* **126** 371
[5] Sakata S and Yamada T 2006 U.S. Patent 7 074 346[P] 2006-7-11
[6] Xie, R J, Hirosaki N, Sakuma K, Yamamoto Y and Mitomo M 2004 *Appl. Phys. Lett.* **84** 5404
[7] Im W B, Fourr Ú Y, Brinkley S, Sonoda J, Nakamura S, DenBaars S P and Seshadri R 2009 *Opt. Express* **17** 22673
[8] Im W B, Fellows N N, DenBaars S P and Seshadri R 2009 *J. Mater. Chem.* **19** 1325
[9] Im W B, George N, Kurzman J, Brinkley S, Mikhailovsky A, Hu J, Chmelka B F, DenBaars S P and Seshadri R 2011 *Adv. Mater.* **23** 2300
[10] Vogt T, Woodward P M, Hunter B A, Prodjosantoso A K and Kennedy B J 1999 *J. Solid State Chem.* **144** 228
[11] Im W B, Fellows N N, DenBaars S P, Seshadri R and Kim Y I 2009 *Chem. Mater.* **21** 2957
[12] Dorenbos P 2000 *J. Lumin.* **91** 155
[13] Dorenbos P 2001 *Phys. Rev. B* **64** 125117
[14] Dorenbos P 2002 *J. Lumin.* **99** 283
[15] Dorenbos P 2003 *J. Lumin.* **105** 117
[16] Li P L, Yang Z P, Wang Z J and Guo L Q 2008 *Chin. Phys. B* **17** 1907
[17] Duan M L, Kuang X Y, Zhang C X and Chai R P 2011 *Chin. Phys. B* **20** 013102
[18] Jiang Z Q, Wang Y H and Guo Y 2010 *Chin. Phys. B* **19** 027801
[19] Özen G, Forte O and Di Bartolo B 2005 *J. Appl. Phys.* **97** 013510
[20] Özen G, Forte O and Di Bartolo B 2005 *Opt. Mater.* **27** 1664
[21] Malinowski M, Szczepanski P, Wolinski W, Wolski R and Frukacz Z 1993 *J. Phys.: Condens. Matter* **5** 6469
[22] Li G G, Peng C, Zhang C M, Xu Z H, Shang M M, Yang D M, Kang X J, Wang W X, Li C X and Cheng Z Y 2010 *Inorg. Chem.* **49** 10522
[23] Shang M M, Li G G, Kang X J, Yang D M, Geng D L and Lin J 2011 *ACS Appl. Mater. & Interfaces* **3** 2738